An explanation for the simulated aborted ENSO events in climate models

Huaxia Liao[1], Yongqiang yong Yu[2], Chunzai Wang[3], Xiang Han[4], and Zhenya Song[5]

[1]South China Sea Institute Of Oceanology
[2]Chinese Academy of Sciences (CAS)
[3]State Key Laboratory of Tropical Oceanography, South China Sea Institute of Oceanology, Chinese Academy of Sciences (CAS)
[4]South China Sea Institute of Oceanology
[5]First Institute of Oceanography, Ministry of Natural Resources, China

November 22, 2022

Abstract

El Niño-Southern Oscillation (ENSO) seasonal phase-locking behaviors simulated in 36 Coupled Model Intercomparison Project Phase 6 (CMIP6) models are evaluated for the first time by comparison with 43 CMIP5 models and observations. There are much more aborted ENSO events (simulated mature phase occurring out of the winter season) in 30 CMIP6 and 33 CMIP5 models than in observations, which indicates that the reasonable ENSO seasonal phase-locking is still a challenge to state-of-the-art climate models. Furthermore, the seasonal cycle of the zonal SST gradient along the equator can explain approximately 30% and 36% of the variance in the ENSO phase locking for CMIP5 and CMIP6, respectively. Moreover, both the spatial distribution and the phase change timing of the zonal SST gradient seasonal cycle are crucial for the ENSO seasonal phase locking. Improvement of the simulating ENSO phase-locking should be realized by focusing on the seasonal cycle of the zonal SST gradient.

Hosted file

`supporting-information_20200308.docx` available at https://authorea.com/users/533828/articles/598321-an-explanation-for-the-simulated-aborted-enso-events-in-climate-models

An explanation for the simulated aborted ENSO events in climate models

Huaxia Liao[1, 2, 3], Yongqiang Yu[3, 4, 5], Chunzai Wang[1, 6, 7], Xiang Han[1, 3], Zhenya Song[2, 8, 9]

[1] State Key Laboratory of Tropical Oceanography, South China Sea Institute of Oceanology, Chinese Academy of Sciences, Guangzhou 510301, China

[2] Laboratory for Regional Oceanography and Numerical Modeling, Qingdao National Laboratory for Marine Science and Technology, Qingdao 266237, China

[3] University of Chinese Academy of Sciences, Beijing 100049, China

[4] State Key Laboratory of Numerical Modeling for Atmospheric Sciences and Geophysical Fluid Dynamics, Institute of Atmospheric Physics, Chinese Academy of Sciences, Beijing 100029, China

[5] Center for Ocean Mega-Science, Chinese Academy of Sciences, Qingdao 266071, China

[6] Southern Marine Science and Engineering Guangdong Laboratory (Guangzhou), Guangzhou 511458, China

[7] Innovation Academy of South China Sea Ecology and Environmental Engineering, Chinese Academy of Sciences, Guangzhou 510000, China

[8] First Institute of Oceanography, Ministry of Natural Resources, Qingdao 266061, China

[9] Key Laboratory of Marine Science and Numerical Modeling, Ministry of Natural Resources, Qingdao 266061, China

Submitted to Geophysical Research Letters

Correspondence to:

Prof. Zhenya Song

Email: songroy@fio.org.cn

Address: No. 6 Xian-Xia-Ling Road, Qingdao 266061, China
Tel: 86-532-88965937

Key Points:

- ENSO seasonal phase-locking behaviors simulated in CMIP5 and CMIP6 are evaluated for the first time.
- Aborted ENSO events (the simulated mature phase tends to occur out of the winter season) still prevail among CMIP5 and CMIP6 models.
- The ability to simulate the realistic seasonal cycle of the zonal SST gradient is crucial to the ENSO phase locking.

Abstract

El Niño-Southern Oscillation (ENSO) seasonal phase-locking behaviors simulated in 36 Coupled Model Intercomparison Project Phase 6 (CMIP6) models are evaluated for the first time by comparison with 43 CMIP5 models and observations. There are much more aborted ENSO events (simulated mature phase occurring out of the winter season) in 30 CMIP6 and 33 CMIP5 models than in observations, which indicates that the reasonable ENSO seasonal phase-locking is still a challenge to state-of-the-art climate models. Furthermore, the seasonal cycle of the zonal SST gradient along the equator can explain approximately 30% and 36% of the variance in the ENSO phase locking for CMIP5 and CMIP6, respectively. Moreover, both the spatial distribution and the phase change timing of the zonal SST gradient seasonal cycle are crucial for the ENSO seasonal phase locking. Improvement of the simulating ENSO phase-locking should be realized by focusing on the seasonal cycle of the zonal SST gradient.

Plain Language Summary

El Niño-Southern Oscillation (ENSO) is the most significant interannual variability on earth and has enormous impacts on the global climate and human livelihood. The ability to forecast ENSO accurately is crucially important. ENSO is characterized by strong peak sea surface temperature (SST) anomalies in the central-eastern tropical Pacific during the mature phase in winter. However, we found that the simulated mature phase of ENSO events still tends to occur out of the winter season (called “aborted ENSO events”) in state-of-the-art climate models by comparing 36 CMIP6 models with 43 CMIP5 models and observations. This tendency can seriously affect the ENSO prediction ability. Further analysis indicates that the seasonal cycle of the zonal SST gradient along the equator, including both the spatial distribution and timing of phase changes, is crucial for ENSO phase locking. Earlier phase changes of the zonal SST gradient from negative to positive in October can lead to aborted ENSO events through the premature reduction of zonal advection and thermocline feedbacks. Furthermore, unrealistic spatial distributions can also change

the seasonal cycle of zonal SST gradient, therefore producing more aborted ENSO events. Our study is instructive for the improvements in ENSO prediction and therefore can greatly benefit our society.

1 Introduction

El Niño-Southern Oscillation (ENSO) is the most prominent interannual climate variability on earth and is characterized by strong winter peaked sea surface temperature (SST) anomalies in the central-eastern tropical Pacific [*Mitchell & Wallace*, 1996; *Neelin et al.*, 2000; *Philander*, 1983; *Wang & Picaut*, 2004]. The ability to forecast ENSO accurately is crucial to the livelihoods of people globally [*Brönnimann et al.*, 2004; *Cai et al.*, 2019; *Wang*, 2019]. A climate model is the key tool to simulate and predict ENSO events. However, simulating reasonable ENSO seasonal phase-locking behavior is still a challenge to climate models. The simulated mature phase of ENSO events (hereafter called "aborted ENSO events") tends to occur out of the winter season [*Balmaseda et al.*, 1995; *Bellenger et al.*, 2014; *Ham & Kug*, 2014]. Failing to simulate the seasonal phase locking of ENSO can severely affect model's ability to simulate tropical climate variability and global monsoons [*Brönnimann et al.*, 2004; *Cai et al.*, 2019].

Many studies have discussed the mechanisms of ENSO seasonal phase locking and the causes of simulation biases. Early studies proposed the dynamics of the nonlinear interaction between the ENSO cycle and the annual cycle based on a simple couple model [*Jin et al.*, 1996; *Neelin et al.*, 2000]. However, the mechanisms are more complicated for climate models. Many climate models experience the double Intertropical Convergence Zone (ITCZ) problem [*Lin*, 2007], with too zonally elongated South Pacific convergence zone (SPCZ) over the southwestern Pacific [*McGregor et al.*, 2012; *McGregor et al.*, 2013]. The biases in simulating the SPCZ prevent the southward shift of the westerly wind in boreal spring, hence disturbing the winter peak tendency of ENSO [*Harrison & Vecchi*, 1999; *Tziperman et al.*, 1997; *Tziperman et al.*, 1998; *Zheng & Yu*, 2007]. In addition to the double ITCZ problem, unrealistic simulations of tropical SST are fundamentally important [*An & Wang*, 2001; *Chen et al.*, 2019; *Ham et al.*, 2012]. The simulated SST represents the conditions in simulating the tropical Pacific zonal SST gradient and thermocline depth. Therefore, it modulates the simulated ENSO cycle through zonal advective and thermocline feedback. Studies have suggested that models with aborted ENSO events tends to simulate colder SST and amplified oceanic feedbacks in boreal summer [*Ham & Kug*, 2014]. The cold biases of SST also lead to weak phase locking by suppressing thermocline feedback and Ekman feedback in boreal winter [*Wengel et al.*, 2018]. In addition to SST, incorrect simulation of shortwave feedback [*Bellenger et al.*, 2014; *Rashid & Hirst*, 2016], as well as the seasonal cycle of the mean current, affect the winter ENSO peak [*Stein et al.*, 2010]. Therefore, even with the above described progress, the explanation of the aborted ENSO events is still inconclusive.

Multimodel analyses have shown only modest improvements in ENSO phase-locking simulation from CMIP3 to CMIP5, and too many aborted ENSO events still represent a common problem in CMIP5 models [*AchutaRao & Sperber*, 2002; *Bellenger et al.*, 2014; *Ham & Kug*, 2014]. More than 30 climate models participating in CMIP6 [*Eyring et al.*, 2016] have recently published their simulation results. These published data provide an excellent opportunity to assess the ENSO phase-locking simulation ability and analyze the reason for aborted ENSO events in state-of-the-art climate models.

This study evaluates the simulated ENSO seasonal phase-locking ability for 43 CMIP5 and 36 CMIP6 models and proposes a possible explanation for the abovementioned ENSO events. A brief description of the datasets and the analysis methods used in this study are presented in section 2. Section 3 evaluates the simulation results and analyze the mechanisms of aborted ENSO events in CMIP5 and CMIP6 models. Section 4 presents the discussion and conclusion.

2 Data and Methodology

2.1 Observational and model datasets

The SST datasets referred to as observations were derived from the Hadley Center Sea Ice and Sea Surface Temperature (HadISST) dataset starting at 1870 on a 1°×1° grid [*Rayner et al.*, 2003] and the Extended Reconstructed Sea Surface Temperature (ERSST) version 5 starting at 1854 on a 2°×2° grid [*Huang et al.*, 2017].

The first realization of the historical simulation from 43 CMIP5 (r1i1p1) and 36

CMIP6 (r1i1p1f1) climate models used in this study are summarized in Table S1 and Table S2. Each historical simulation was integrated from a pre-industrial control simulation spin-up experiment and then forced by solar, volcanic, aerosol, and greenhouse gas data from 1850 to 2005 for the CMIP5 historical experiments [*Taylor et al.*, 2012] and from 1850 to 2014 for the CMIP6 historical experiments [*Eyring et al.*, 2016].

In this study, we select the monthly outputs from 1870 to 2005 based on both observations and model results for analysis. All of the data were interpolated to a 1°×1° grid.

2.2 Methods

The El Niño and La Niña events were defined by using the SST anomaly averaged over the Niño3 region (150°W-90°W, Niño3 index). In each observation and model, we define El Niño and La Niña events as periods when the Niño3 index exceeds half of its standard deviation (SD) for over six months [*Levine et al.*, 2016]. For each Niño3 index, preprocessing of the long-term linear detrend [*Lindsey*, 2013] and three-month running average were used before calculating the El Niño (La Niña) events.

The seasonal cycle was calculated by removing the annual mean value from the climatology. The correlation coefficients of the seasonal cycle between each model and observations were used to evaluate the simulation performance of the seasonal cycle.

In this paper, we define the concept of "aborted El Niño (La Niña) events" [*Guilyardi et al.*, 2003] as El Niño (La Niña) events that were aborted during the development processes and peaked before winter (March to September). Because of the similar mechanisms in the evolution of El Niño and La Niña events, we used aborted El Niño events to classify the simulation ability in terms of ENSO phase-locking in each model.

Based on the proportions of aborted El Niño events out of all El Niño events, we classified the models into three categories (Figures 1b and 1c). The model was classified as Aborted_L if the proportion of aborted El Niño events was under 1/3. If the proportion exceeded 2/3, the model was classified as Aborted_H. The rest of the models were marked as Aborted_M. The robust features of the ensemble were examined by its intermodel SD [*Jia et al.*, 2019].

In this study, we found that the simulated ENSO usually peaked randomly in each month (Figure S1) when climate models failed to simulate the seasonal cycle of the zonal SST gradient in the central-eastern Pacific (2°S-2°N, 180°-100°W). The correlation coefficients between the observations and simulations in these models were smaller than 0.576, which corresponded to the 95% significance level based on a two-tailed Student's t-test. The proportion of the aborted El Niño events in these models was close to 2/3 (7 months out of a total of 12 calendar months), which caused confusion in the characteristics of the Aborted_M and Aborted_H models. Therefore, these models were neglected in the multimodel ensemble analyses. Furthermore, the climate models failed in simulating the seasonal cycle of the SST in the eastern Pacific (2°S-2°N, 150°-90°W) are showed in Figure S2.

3 Results

3.1 Model assessment

In the observations, ENSO presents strong phase locking with a maximum SST anomaly variability in winter and a minimum SST anomaly variability in spring [*An & Wang*, 2001; *Bellenger et al.*, 2014]. Seasonality diagnosis shows that both the CMIP5 and CMIP6 ensemble means can capture the basic states of the observed seasonal ENSO variability (Figure 1a). The CMIP6 model ensemble mean shows larger standard deviations in each calendar month than the observation and CMIP5 model ensemble means, which may reflect the larger amplitudes of several models, such as CESM2-FV2. However, the seasonal phase locking of both the CMIP5 and CMIP6 ensemble means is weaker than that of observations. There are also large intermodel variabilities in the CMIP5 and CMIP6 ensembles, indicating that ENSO in individual models may peak in any season. Sixteen CMIP5 models (37% of the 43 models) and 18 CMIP6 models (50% of the 36 models) show a maximum standard deviation in the SST anomaly in November-January, which indicates that the ability to simulate ENSO seasonal phase locking improves from CMIP5 to CMIP6. However, there is still room for additional improvement.

To further evaluate the ability to simulate the ENSO phase locking in each model, we propose the concept of “aborted El Niño events” (see Methods). The proportions of the aborted El Niño events are 0.15 (5 out of 34 total El Niño events) in the ERSST dataset and 0.23 (7 out of 31 total El Niño events) in the HadISST dataset. Based on the proportions of the aborted El Niño events out of all El Niño events, we classify the models into three categories (Figures 1b and 1c, Table S1 and S2). Aborted_L represents models with relatively realistic ENSO phase locking, such as CESM2-WACCM and FIO-ESM2 in CMIP6 (Figure 1c, Table S2). In contrast, the models that failed to simulate the winter ENSO peak are identified as Aborted_H models. Ten out of 43 (approximately 23%) CMIP5 models are Aborted_L models (Figure 1c, Table S1), while only 6 out of 36 (approximately 17%) CMIP6 models are classified as Aborted_L (Figure 1b, Table S2). It seems there is no improvement in simulating the ENSO phase locking from CMIP5 to CMIP6 based on the numbers of Aborted_L models. The stalled progress may relate to the progress of CMIP6, since some Aborted_L models in CMIP5 (e.g., the models from the Hadley Center in the UK) have been unavailable until now. Moreover, there are clear improvements in CMIP6 if the Aborted_L model threshold is increased slightly. Specifically, 12 out of 43 (approximately 28%) CMIP5 and 14 out of 36 (approximately 0.39%) CMIP6 models are classified as Aborted_L if we increase the threshold of the Aborted_L model from 0.37 to 0.4. Clear improvements are also found in some individual models, such as the models from the Geophysical Fluid Dynamics Laboratory in USA, which are classified as Aborted_L if the threshold is increased. We suggest that the ENSO seasonal phase locking is modestly improved from CMIP5 to CMIP6.

3.2 Phase-locking simulation bias analysis

Several studies [*Jin & An*, 1999; *Wang & Picaut*, 2004; *Zhu et al.*, 2015] have suggested that the evolution of ENSO is dominated by zonal advective feedback and thermocline feedback, which are highly connected to the zonal gradient of SST in the central-eastern tropical Pacific and the thermocline depth in the eastern Pacific. The realistic simulation of the zonal SST gradient is crucial to the simulation of the ENSO seasonal phase locking [*An & Wang*, 2001; *Ham & Kug*, 2014]. Changes in the zonal SST gradient modulate the strength of the zonal advective feedback. Furthermore, the seasonal changes in the zonal SST gradient associated with the changes in thermocline depth in the eastern tropical Pacific [*Karnauskas et al.*, 2009; *Zhu et al.*, 2015] reflect changes in the thermocline feedback strength. Figure 2 presents the simulated and observed seasonal cycle of the zonal SST gradient in the equatorial Pacific. The observed zonal gradient of SST turns positive after January and then reverses to negative after July, with the maximum amplitude spreading uniformly over the central-eastern equatorial Pacific (180°-100°W, Figure 2d). The negative zonal SST gradient amplifies the zonal SST variation in the equatorial Pacific and vice versa. Therefore, the strengths of the zonal advective feedback and thermocline feedback increase from January to June and decrease from July to December. The seasonal cycle of the zonal SST gradient turns from negative to positive in January. Thus, ENSO can develop rapidly in boreal summer and autumn but decays in subsequent spring due to changes in zonal advection and the thermocline feedback strength.

Similar to the observations, all three categories of the model ensemble mean present a clear seasonal cycle of the zonal SST gradient in the equatorial Pacific (Figure 2a-2c). However, there are also apparent differences between these categories (Figure 2e-2f). The models that are poor in simulating the winter El Niño peak (Aborted_M and Aborted_H) tend to simulate an earlier phase change in October. The earlier phase changes of the seasonal zonal SST gradient from negative to positive in October can lead to earlier peaks of the simulated El Niño events in the Aborted_H models. The effects of these unrealistic phase changes are more obvious in individual models than in ensemble means. For example, the seasonal cycle of the zonal SST gradient in the CESM2-FV2 model reverses from the negative to positive phases in October (Figure S3a). In response to the earlier phase change, all of the aborted El Niño events in CESM2-FV2 (15 out of 39 total El Niño events) peak in late summer (July August-September). In contrast, the HadGEM2-CC model shows delayed phase changes of the seasonal zonal SST gradient in boreal spring (Figure S3b). Thus, approximately two-thirds of the aborted El Niño events (16 out of 24 aborted El Niño events) in the HadGEM2-CC model peak in spring (March-April-May).

The ensemble means of the three categories also show that a model that fails to simulate the winter El Niño peak (Aborted_M and Aborted_H) tends to simulate a weaker seasonal cycle of the zonal SST gradient (Figure 2). We found that the weaker amplitudes of the Aborted_M and Aborted_H ensemble means are highly connected to the spatial patterns of the seasonal zonal SST gradient in some models. A model with realistic zonal spatial distributions and phase changes of the zonal SST gradient over the central-eastern equatorial Pacific (180°-100°W), such as CESM-CAM5 (Figure S3c) in Aborted_L ensembles, tends to simulate the winter ENSO peak well. Furthermore, the proportion of aborted El Niño events is close to or exceeds two-thirds in models with an inaccurate zonal spatial distribution, such as CMCC-CM (Figure S3d), MRI-ESM1 and MPI-ESM1-2-HR, which fail to simulate the winter ENSO peak. Unlike the uniformly spread zonal SST gradient in observations, the unrealistic and discontinuous spatial distribution weakens the amplitude and disturbs the phase changes of the zonal SST gradient seasonal cycle. Therefore, this unrealistic distribution affects the seasonal changes in zonal advective feedback and thermocline feedback strength and eventually changes the simulated ENSO phase locking. There is high diversity among the models with inaccurate zonal spatial distributions. The zonal spatial distribution biases in those models are complicated and may cancel each other. Thus, the amplitudes of the seasonal zonal SST gradient in the Aborted_M and Aborted_H ensemble means are much weaker than the amplitude in the Aborted_L ensemble mean.

We suggest that both the spatial distribution and the phase change timing of the seasonal zonal SST gradient are crucial for the ENSO phase locking. However, these two factors are complicated and usually tangled in individual models. It is challenging to examine the exact contributions of each factor. Thus, the spatial distribution and the phase changes have a combined effect on the simulation ability of the seasonal zonal SST gradient. In this study, we define the accuracy of the zonal SST gradient seasonal cycle as the correlation between the observed and simulated zonal mean of the seasonal zonal SST gradient over the central-eastern equatorial Pacific (180°-100°W), where the observed seasonal cycle of the zonal SST gradient is uniformly and stably spread.

To shed further light on the mechanisms of the simulated ENSO seasonal phase locking, scatter plots are used to determine the connections between the proportion of the simulated aborted El Niño events out of all El Niño events and the accuracy of the simulated zonal SST gradient seasonal cycle in the central-eastern equatorial Pacific (Figure 3). The multiple correlation coefficients based on CMIP5 and CMIP6 are 0.54 and 0.60, respectively, which correspond to approximately 30% and 36% of the explained variance, respectively. In addition, the multiple correlation coefficients increase from CMIP5 to CMIP6. This enhancement of the multiple correlation coefficients highlights the importance of the seasonal cycle of the zonal SST gradient in state-of-the-art climate models and suggest that decreased biases in the simulation of other processes are due to the decrease in the residual explained variances. Note that the correspondences remain stable even when we change the boundary of the zonal SST gradient slightly. Hence, we suggest that the ability to simulate the seasonal cycle of the equatorial Pacific zonal SST gradient realistically is essential in simulating the ENSO seasonal phase locking.

4 Conclusions and Discussion

This study examined the ENSO seasonal phase locking based on 43 CMIP5 and 36 CMIP6 models, showing that the simulation of reasonable ENSO seasonal phase-locking behavior is still a challenge to CMIP6 models. We found that the seasonal cycle of the zonal SST gradient along the equator, including both the spatial distribution and the timing of phase changing, is crucial for the ENSO phase locking. The realistic simulation of the zonal SST gradient improves the spatial distribution and phase changing timing of the simulated zonal advection and thermocline feedback, which both dominate the evolution of ENSO events. Unlike previous studies, our research suggests that the realistic simulation of the zonal SST gradient rather than the SST is essential in simulating the ENSO seasonal phase locking. The examination of local SST is unable to reflect the thermal difference along the equator and thus may neglect seasonal changes in equatorial trade wind strength, as well as the associated horizontal advection and thermocline process. The correlation coefficients between the proportion of simulated aborted El Niño events out of all El Niño events and the accuracy of the simulated SST seasonal cycle in the eastern equatorial Pacific region are 0.23 and 0.37 based on CMIP5 and CMIP6, respectively (Figures S4), which correspond to approximately 10% of the explained variance. Some models, such as ACCESS-CM2 in CMIP6, demonstrate very poor behavior in simulating the seasonal cycle of SST but have excellent performances in simulating the zonal SST gradient and the winter peaked El Niño (Figures S5a and S5d).

It should be noted that the effectiveness of diagnoses through the accuracy of seasonal zonal SST gradients may be low in certain situations. For example, the MAM-UA-1-0 model can generally simulate the amplitude and phase change timing of the seasonal zonal SST gradient (Figures S5b and S5e). However, the simulated zonal SST gradient decreases suddenly in October, accompanied by abrupt changes in zonal advection and thermocline feedback. Thus, most of the aborted El Niño events in MAM-UA-1-0 peak in August and September. Therefore, caution should be taken when analyzing the ENSO seasonal phase locking in a single model.

Some previous studies suggest that a model that fails to simulate the winter peak of ENSO tends to simulate enhanced zonal advective and thermocline feedback in boreal summer, which is opposite to our results. The difference may be due to the different datasets we use. Ham and Kug (2014) use 21 CMIP3 and 21 CMIP5 models as an ensemble, while we use 43 CMIP5 and 36 CMIP6 models. Our conclusions are not conflicting since individual models may exhibit excessive summer zonal SST gradients and earlier phase changes together (Figure S3a). We also check the simulated ENSO seasonal phase locking through El Niño events based on the Niño3.4 index (Figure S6) and through La Niña events based on the Niño3 index (Figure S7). Both show clear connections between the proportion of simulated aborted ENSO events out of all ENSO events and the accuracy of the simulated seasonal cycle of the zonal SST gradient, revealing that the ability to simulate the seasonal cycle of the zonal SST gradient is essential in simulating ENSO seasonal phase locking.

The seasonal cycle of the zonal SST gradient can explain approximately 30% to 36% of the variance in the simulated El Niño seasonal phase locking. In other words, 60% to 70% of the variability remains unaccounted for by this approach. For example, INM-CM5-0 is a member of the Aborted_L model but failed to simulate the realistic seasonal cycle of the zonal SST gradient (Figure S1). The residual variability may be due to other problems, such as an excessive summer zonal SST gradient [*Ham & Kug*, 2014], the double ITCZ problem [*Zheng & Yu*, 2007; *McGregor et al.*, 2012] and shortwave feedback bias [*Bellenger et al.*, 2014]. In addition, the simulated mean thermocline depth in the eastern equatorial Pacific limits the variations in the anomalous thermocline depth [*Wengel et al.*, 2018; *Zhu et al.*, 2015], thus disturbing the linkages between the seasonal cycle of the zonal SST gradient and thermocline depth. Further analyses should be performed in future studies.

Acknowledgements

This work was supported by the National Key R&D Program of China (2016YFA0602200 and 2019YFA0606701), the Basic Scientific Fund for the National Public Research Institute of China (2016S03), the National Natural Science Foundation of China (41821004, 41731173, 41530426 and 91958201), the Strategic Priority Research Program of Chinese Academy of Sciences (XDA19060102), the AoShan Talents Cultivation Excellent Scholar Program Supported by Qingdao National Laboratory for Marine Science and Technology (2017ASTCP-ES04), the

China-Korea Cooperation Project on Northwestern Pacific Climate Change and its Prediction, and the Pioneer Hundred Talents Program of the Chinese Academy of Sciences, the Leading Talents of Guangdong Province Program. We acknowledge the World Climate Research Programme, which, through its Working Group on Coupled Modelling, coordinated and promoted CMIP5 and CMIP6. We thank the climate modeling groups for producing and making available their model output, the Earth System Grid Federation (ESGF) for archiving and providing access to data, and the multiple funding agencies who support CMIP and ESGF. All CMIP data in this study are available from https://doi.org/10.6084/m9.figshare.11977938.v2, which were downloaded from the ESGF website and then interpolated to a 1x1 grid. The HadISST and ERSST datasets are from the Met Office Hadley Center (https://www.metoffice.gov.uk/hadobs/hadisst/data/download.html) and NCDC/NOAA (https://www1.ncdc.noaa.gov/pub/data/cmb/ersst/v5/netcdf/), respectively.

References

AchutaRao, K., and Sperber, K. (2002), Simulation of the El Niño Southern Oscillation: Results from the coupled model intercomparison project, *Climate Dynamics*, *19*(3-4), 191-209. doi:https://doi.org/10.1007/s00382-001-0221-9

An, S.-I., and Wang, B. (2001), Mechanisms of locking of the El Niño and La Niña mature phases to boreal winter, *Journal of climate*, *14*(9), 2164-2176.

doi:https://doi.org/10.1175/1520-0442(2001)014<2164:MOLOTE>2.0.CO;2

Balmaseda, M. A., Davey, M. K., and Anderson, D. L. (1995), Decadal and seasonal dependence of ENSO prediction skill, *Journal of Climate*, *8*(11), 2705-2715. doi:https://doi.org/10.1175/1520-0442(1995)008<2705:dasdoe>2.0.co;2

Bellenger, H., Guilyardi, É., Leloup, J., Lengaigne, M., and Vialard, J. (2014), ENSO representation in climate models: From CMIP3 to CMIP5, *Climate Dynamics*, *42*(7-8), 1999-2018. doi:https://doi.org/10.1007/s00382-013-1783-z

Brönnimann, S., Luterbacher, J., Staehelin, J., Svendby, T., Hansen, G., and Svenøe, T. (2004), Extreme climate of the global troposphere and stratosphere in 1940–42 related to El Niño, *Nature*, *431*(7011), 971-974. doi:https://doi.org/10.1038/nature02982

Cai, W., Wu, L., Lengaigne, M., Li, T., McGregor, S., Kug, J.-S., *et al.* (2019), Pantropical climate interactions, *Science*, *363*(6430), eaav4236. doi:10.1126/science.aav4236

Chen, X., Liao, H., Lei, X., Bao, Y., and Song, Z. (2019), Analysis of ENSO simulation biases in FIO-ESM version 1.0, *Climate Dynamics*, *53*(11), 6933-6946. doi:https://doi.org/10.1007/s00382-019-04969-w

Eyring, V., Bony, S., Meehl, G. A., Senior, C. A., Stevens, B., Stouffer, R. J., and Taylor, K. E. (2016), Overview of the Coupled Model Intercomparison Project Phase 6 (CMIP6) experimental design and organization, *Geoscientific Model Development*, *9*(LLNL-JRNL-736881).

doi:https://doi.org/10.5194/gmd-9-1937-2016

Guilyardi, E., Delecluse, P., Gualdi, S., and Navarra, A. (2003), Mechanisms for ENSO phase change in a coupled GCM, *Journal of climate*, *16*(8), 1141-1158. doi:https://doi.org/10.1175/1520-0442(2003)16<1141:mfepci>2.0.co;2

Ham, Y.-G., and Kug, J.-S. (2014), ENSO phase-locking to the boreal winter in CMIP3 and CMIP5 models, *Climate dynamics*, *43*(1-2), 305-318. doi:https://doi.org/10.1007/s00382-014-2064-1

Ham, Y.-G., Kug, J.-S., Kim, D., Kim, Y.-H., and Kim, D.-H. (2012), What controls phase-locking of ENSO to boreal winter in coupled GCMs?, *Climate dynamics*, *40*(5-6), 1551-1568. doi:https://doi.org/10.1007/s00382-012-1420-2

Harrison, D., and Vecchi, G. A. (1999), On the termination of El Niño, *Geophysical Research Letters*, *26*(11), 1593-1596. doi:https://doi.org/10.1029/1999gl900316

Huang, B., Thorne, P. W., Banzon, V. F., Boyer, T., Chepurin, G., Lawrimore, J. H., *et al.* (2017), Extended reconstructed sea surface temperature, version 5 (ERSSTv5): upgrades, validations, and intercomparisons, *Journal of Climate*, *30*(20), 8179-8205. doi:https://doi.org/10.1175/jcli-d-16-0836.1

Jia, F., Cai, W., Wu, L., Gan, B., Wang, G., Kucharski, F., *et al.* (2019), Weakening Atlantic Niño–Pacific connection under greenhouse warming, *Science advances*, *5*(8), eaax4111. doi:https://doi.org/10.1126/sciadv.aax4111

Jin, F.-F., and An, S. I. (1999), Thermocline and zonal advective feedbacks within the equatorial ocean recharge oscillator model for ENSO, *Geophysical research* *letters*, *26*(19), 2989-2992. doi:https://doi.org/10.1029/1999gl002297

Jin, F.-F., Neelin, J. D., and Ghil, M. (1996), El Nino/Southern Oscillation and the annual cycle: Subharmonic frequency-locking and aperiodicity, *Physica D: Nonlinear Phenomena*, *98*(2-4), 442-465. doi:https://doi.org/10.1016/0167-2789(96)00111-x

Karnauskas, K. B., Seager, R., Kaplan, A., Kushnir, Y., and Cane, M. A. (2009), Observed strengthening of the zonal sea surface temperature gradient across the equatorial Pacific Ocean, *Journal of Climate*, *22*(16), 4316-4321.

Levine, A., Jin, F.-F., and McPhaden, M. J. (2016), Extreme noise–extreme El Niño: How state-dependent noise forcing creates El Niño–La Niña asymmetry, *Journal of Climate*, *29*(15), 5483-5499. doi:https://doi.org/10.1175/jcli-d-16-0091.1

Lin, J.-L. (2007), The double-ITCZ problem in IPCC AR4 coupled GCMs: Ocean–atmosphere feedback analysis, *Journal of Climate*, *20*(18), 4497-4525. doi:https://doi.org/10.1175/jcli4272.1

Lindsey, R. (2013), In watching for El Nino and La Nina, NOAA adapts to global warming, National Oceanic and Atmospheric Administration, Climate Watch Magazine, NOAA Climate.gov, United States.

McGregor, S., Timmermann, A., Schneider, N., Stuecker, M. F., and England, M. H. (2012), The effect of the South Pacific convergence zone on the termination of El Niño events and the meridional asymmetry of ENSO, *Journal of Climate*, *25*(16), 5566-5586. doi:https://doi.org/10.1175/jcli-d-11-00332.1

McGregor, S., Ramesh, N., Spence, P., England, M. H., McPhaden, M. J., and Santoso, A. (2013), Meridional movement of wind anomalies during ENSO events and their role in event termination, *Geophysical Research Letters*, *40*(4), 749-754. doi:https://doi.org/10.1002/grl.50136

Mitchell, T. P., and Wallace, J. M. (1996), ENSO Seasonality: 1950–78 versus 1979–92, *Journal of climate*, *9*(12), 3149-3161. doi:https://doi.org/10.1175/1520-0442(1996)009<3149:ESV>2.0.CO;2.

Neelin, J. D., Jin, F.-F., and Syu, H.-H. (2000), Variations in ENSO phase locking, *Journal of Climate*, *13*(14), 2570-2590. doi:https://doi.org/10.1175/1520-0442(2000)013<2570:viepl>2.0.co;2

Philander, S. G. H. (1983), El Nino southern oscillation phenomena, *Nature*, *302*(5906), 295-301. doi:https://doi.org/10.1038/302295a0

Rashid, H. A., and Hirst, A. C. (2016), Investigating the mechanisms of seasonal ENSO phase locking bias in the ACCESS coupled model, *Climate dynamics*, *46*(3-4), 1075-1090. doi:https://doi.org/10.1007/s00382-015-2633-y

Rayner, N., Parker, D. E., Horton, E., Folland, C. K., Alexander, L. V., Rowell, D., *et al.* (2003), Global analyses of sea surface temperature, sea ice, and night marine air temperature since the late nineteenth century, *Journal of Geophysical Research: Atmosphe*, *108*(D14). doi:https://doi.org/10.1029/2002jd002670

Stein, K., Schneider, N., Timmermann, A., and Jin, F.-F. (2010), Seasonal synchronization of ENSO events in a linear stochastic model, *Journal of climate*, *23*(21), 5629-5643. doi:https://doi.org/10.1175/2010jcli3292.1

Taylor, K. E., Stouffer, R. J., and Meehl, G. A. (2012), An overview of CMIP5 and the experiment design, *Bulletin of the American Meteorological Society*, *93*(4), 485-498. doi:https://doi.org/10.1175/bams-d-11-00094.1

Tziperman, E., Zebiak, S. E., and Cane, M. A. (1997), Mechanisms of seasonal–ENSO interaction, *Journal of the atmospheric sciences*, *54*(1), 61-71. doi:https://doi.org/10.1175/1520-0469(1997)054<0061:mosei>2.0.co;2

Tziperman, E., Cane, M. A., Zebiak, S. E., Xue, Y., and Blumenthal, B. (1998), Locking of El Nino's peak time to the end of the calendar year in the delayed oscillator picture of ENSO, *Journal of climate*, *11*(9), 2191-2199. doi:https://doi.org/10.1175/1520-0442(1998)011<2191:loenos>2.0.co;2

Wang, C. (2019), Three-ocean interactions and climate variability: a review and perspective, *Climate Dynamics*, *53*(7-8), 5119-5136. doi:https://doi.org/10.1007/s00382-019-04930-x

Wang, C., and Picaut, J. (2004), Understanding ENSO physics—A review, *Earth's Climate*, *147*, 21-48. doi:https://doi.org/10.1029/147gm02

Wengel, C., Latif, M., Park, W., Harlaß, J., and Bayr, T. (2018), Seasonal ENSO phase locking in the Kiel Climate Model: The importance of the equatorial cold sea surface temperature bias, *Climate dynamics*, *50*(3-4), 901-919. doi:https://xs.scihub.ltd/https://doi.org/10.1007/s00382-017-3648-3

Zheng, W., and Yu, Y. (2007), ENSO phase-locking in an ocean-atmosphere coupled model FGCM-1.0, *Advances in Atmospheric Sciences*, *24*(5), 833-844. doi:https://xs.scihub.ltd/https://doi.org/10.1007/s00376-007-0833-z

Zhu, J., Kumar, A., and Huang, B. (2015), The relationship between thermocline depth and SST anomalies in the eastern equatorial Pacific: Seasonality and decadal variations, *Geophysical Research Letters*, *42*(11), 4507-4515. doi:https://doi.org/10.1002/2015GL064220

Figures

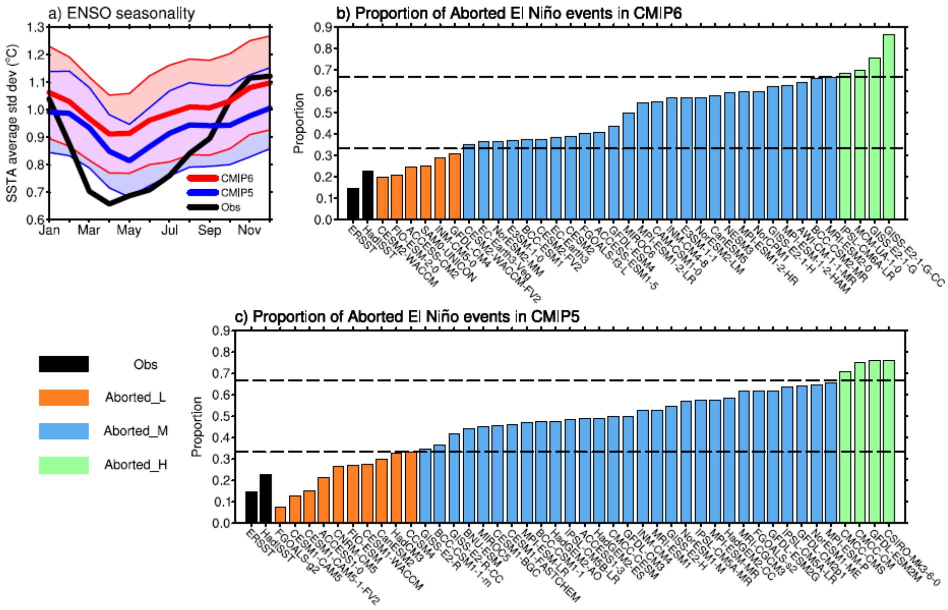

Figure 1. ENSO seasonality diagnoses based on the Niño3 index: (a) Monthly average standard deviation of the Niño3 SST anomalies (°C) for the ERSST (black), CMIP5 (blue) and CMIP6 (red) ensemble means. Classification of Aborted_L (orange), Aborted_M (light blue), and Aborted_H (light green) models based on the proportion of aborted El Niño events for (b) CMIP6 and (c) CMIP5 models. The light color in (a) represent 0.5 times the intermodel SD. The black dashed lines in (b) and (c) represent the 1/3 and 2/3 thresholds, respectively.

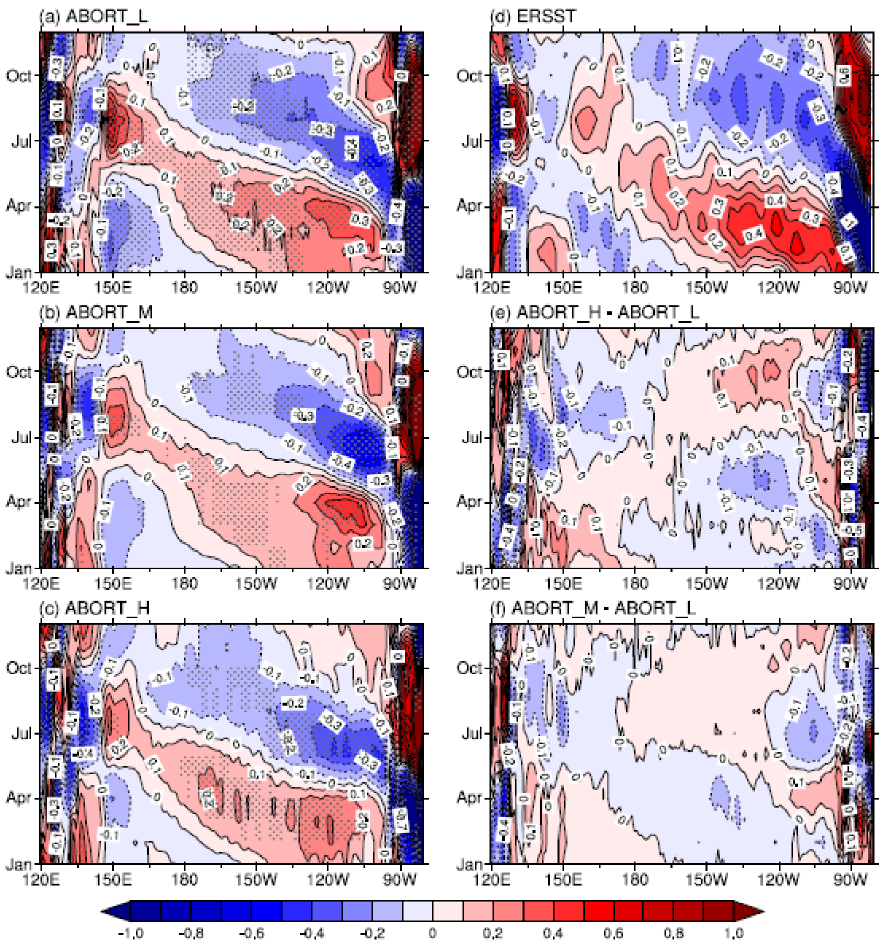

Figure 2. Seasonal cycle of the zonal SST gradient (10^{-6} °C/m) at the equator (2°S-2°N) in the Pacific Ocean for observations (ERSST) and models (ensemble mean of CMIP5 and CMIP6 models). (a) Aborted_L, (b) Aborted_M, (c) Aborted_H, (d) ERSST, (e) Aborted_H - Aborted_L, (e) Aborted_M - Aborted_L. The most robust features of the ensemble where the mean exceeds 1 SD in (a), (b), and (c) are shaded. The models that failed to simulate the seasonal cycle of the zonal SST gradient in the central-eastern equatorial Pacific area (2°S-2°N, 180°-100°W) were neglected.

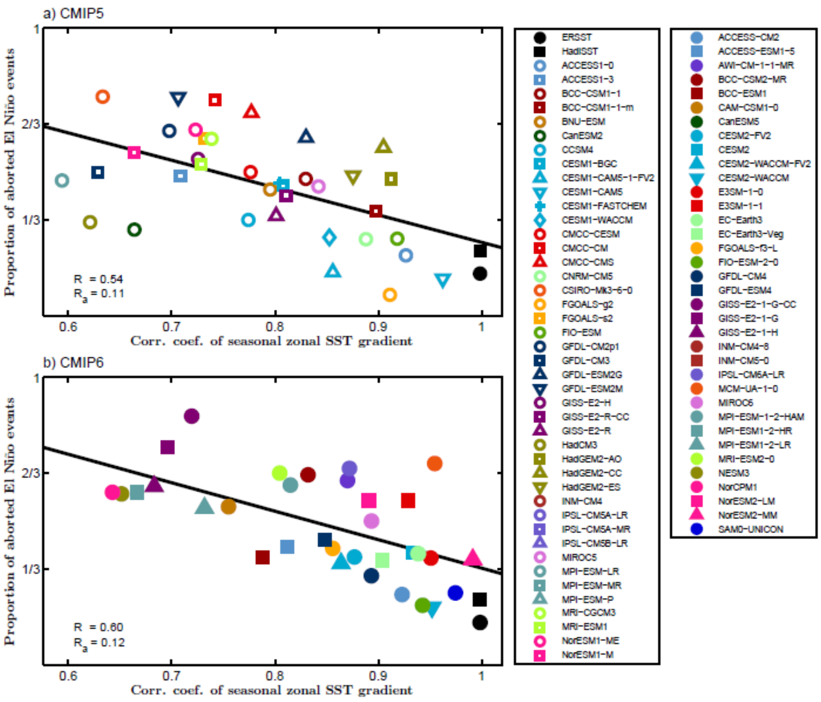

Figure 3. Scatter plots of the simulated El Niño seasonal phase locking and the simulated seasonal cycle of the zonal SST gradient over the equatorial central-east Pacific Ocean (2°S-2°N, 180°-100°W) based on (a) CMIP5 and (b) CMIP6. The X-axis shows the correlation coefficients between the model-simulated and observational seasonal cycles of the zonal SST gradient over the equatorial central-east Pacific Ocean. The Y-axis shows the proportions of aborted El Niño events out of all El Niño events. The black dots represent observations. The solid lines indicate regressions based on the simulated results for which the correlation coefficients are above 0.576. R represents the multiple correlation coefficient of the regression analysis. R_a represents the threshold value of the multiple correlation coefficient at the 99% confidence level based on the F-test.